

Article

Impact of Inter-Regional Transport in a Low-Emission Scenario on PM_{2.5} in Hubei Province, Central China

Jie Xiong ¹, Yongqing Bai ^{1,*}, Tianliang Zhao ^{2,*}, Shaofei Kong ³ and Weiyang Hu ²

¹ Hubei Key Laboratory for Heavy Rain Monitoring and Warning Research, Institute of Heavy Rain, China Meteorological Administration, Wuhan 430205, China; xiongjie8707@sina.com

² Key Laboratory for Aerosol-Cloud-Precipitation of China Meteorological Administration, Nanjing University of Information Science and Technology, Nanjing 210044, China; wyhu_aca@126.com

³ Department of Atmospheric Science, School of Environmental Studies, China University of Geosciences, Wuhan 430074, China; kongshaofei@cug.edu.cn

* Correspondence: 2007byq@163.com (Y.B.); josef_zhao@126.com (T.Z.)

Abstract: In 2020, when the novel coronavirus disease 2019 (COVID-19) broke out as a global pandemic, cities in Hubei Province first went into lockdown on 23 January and resumed work and production on 20 March. From February to March 2020, human activities in Hubei decreased significantly, with the average particulate matter smaller than 2.5 μm (PM_{2.5}) concentration standing at 40 $\mu\text{g}/\text{m}^3$, which is 21% lower than the expected based on a linear fitting trend in the PM_{2.5} concentration in Hubei. By using the empirical orthogonal function (EOF) method, this paper comparatively analyzes the spatial-temporal variations of Hubei's PM_{2.5} concentration anomaly in February and March 2020 and the same periods of 2016–2019. The results show that the daytime peak of the PM_{2.5} daily variation in Hubei in a low-emission scenario during COVID-19 declined significantly, to which human activities contributed the most. However, during nighttime, the PM_{2.5} peak became more prominent, and the meteorological conditions had a more noticeable effect on the PM_{2.5} concentration. In addition, during COVID-19, there was a great drop in PM_{2.5} pollution accumulated from local sources within the urban circle of Wuhan City, while an increase was seen in central-western Hubei due to the inter-regional pollutant transport. Thus, the high PM_{2.5} concentration center in the urban circle of Wuhan disappeared, but the pollution transport channel cities in central-western Hubei remained as high-PM_{2.5}-concentration centers.

Keywords: COVID-19; PM_{2.5}; inter-regional transport; spatial-temporal variation; empirical orthogonal function (EOF)



Citation: Xiong, J.; Bai, Y.; Zhao, T.; Kong, S.; Hu, W. Impact of Inter-Regional Transport in a Low-Emission Scenario on PM_{2.5} in Hubei Province, Central China. *Atmosphere* **2021**, *12*, 250. <https://doi.org/10.3390/atmos12020250>

Received: 30 December 2020

Accepted: 8 February 2021

Published: 13 February 2021

Publisher's Note: MDPI stays neutral with regard to jurisdictional claims in published maps and institutional affiliations.



Copyright: © 2021 by the authors. Licensee MDPI, Basel, Switzerland. This article is an open access article distributed under the terms and conditions of the Creative Commons Attribution (CC BY) license (<https://creativecommons.org/licenses/by/4.0/>).

1. Introduction

During the Spring Festival holiday in 2020, the abrupt outbreak of the coronavirus disease 2019 (COVID-19) pandemic produced unprecedented societal impacts on China. To curb the virus spread among humans, a preventive lockdown was first implemented on January 23 in Wuhan, Hubei. Other major cities/counties in China subsequently followed suit. Due to the restriction measures [1] and Spring Festival effects [2], many factories were shut down, the traffic volume on roads and construction activities reduced obviously, and fireworks were banned, especially in urban regions, etc. The substantial decrease in human activities lessened the anthropogenic emission and thus improved the air quality [3]. Up to 90% reduction in certain emissions during the city lockdown period can be identified from satellite and ground-based observations [4]. The absence of motor vehicles and suspended manufacturing during the COVID-19 pandemic in China created a unique test to assess the efficiency of air pollution mitigation and provided a possibility for revealing the refined spatial-temporal characteristics of air pollution and the impact of meteorological conditions in a low-emission scenario (LES). Many studies have reported changes in air pollutants because of the COVID-19 pandemic [1,5–11] but have not involved the variation

of inter-regional pollutants. Now, we are to focus on the inter-regional transport in the LES during the COVID-19 lockdown period in Hubei Province of Central China.

Atmospheric particulate matters have a long retention time in the air and a wide range of influence, especially those smaller than $2.5\ \mu\text{m}$ ($\text{PM}_{2.5}$). They can stay in the air for a few weeks, covering a large area and a long distance, so they have an obvious inter-regional transport effect [12–14]. The influence of inter-regional $\text{PM}_{2.5}$ transport and surrounding pollution sources has become the key link and hotspot research problem to be urgently solved [15]. In North China, the rapid generation and elimination changes of extreme haze events in Beijing are mainly caused by regional transport and north–south air mass alternation [16,17]. The regional transport contribution of $\text{PM}_{2.5}$ was estimated to be as high as 53–70%, showing explosive growth [18]. The southwest and southeast channels are the main channels to transport pollutants and water vapor to the Beijing–Tianjin–Hebei region, providing material and water vapor conditions for the occurrence and development of haze [19]. In addition, inter-regional transport has made critical contributions to the pollutions in many places such as East China [20] and South China [14].

Hubei Province, located downwind of the East Asian winter monsoon over the heavy-haze-pollution areas of North China, Central Plain of China, and East China, is an important hub for the regional transport of air pollutants over the central-eastern parts of China. At the same time, this region has registered an abnormal, sudden increase in atmospheric aerosol, becoming a new regional haze pollution center [21]. Research shows that the cold air activity causes the inter-regional transport of atmospheric pollutants over the central-eastern parts of China, very easily bringing about the convergence effect over the middle reach of the Yangtze River [22]. The $\text{PM}_{2.5}$ concentration tends to increase rapidly by the action of strong north winds in Hubei, and pollution transport across the urban clusters plays an important role in the formation of heavy haze pollution in this region [23].

Hubei's lockdown in 2020 lasted for almost two months (lockdown on 23 January onward and resuming work on 20 March). Compared to the situation in the same period in 2019, the emission reduction reached 92% [3]. This paper is to study what differences exist in the spatial-temporal distribution of $\text{PM}_{2.5}$ in Hubei between the 2020 lockdown period and the previous years and how the pollutants that were transported from other regions affected the $\text{PM}_{2.5}$ concentration in Hubei in the LES. Therefore, by using the environmental and meteorological observation data of Hubei Province and the empirical orthogonal function (EOF) method, this paper decomposes and obtains stable $\text{PM}_{2.5}$ spatial-temporal feature vectors in February and March of 2016–2020. Besides, the impact of meteorological conditions on $\text{PM}_{2.5}$ pollution and the effect of inter-regional $\text{PM}_{2.5}$ transport in Hubei during COVID-19 in the LES is analyzed. The research findings could provide good references for further improving the air quality condition in Hubei in the future.

This paper is organized as follows: Section 2 introduces observation data, method, and numerical experiments conducted in this paper, Section 3 presents the results of the spatial-temporal variation of the $\text{PM}_{2.5}$ concentration in the LES in Hubei Province, and Section 4 manifests the brief conclusions.

2. Data and Methods

2.1. Data Source

February and March were selected to represent the lockdown period in 2020. The hourly statistical $\text{PM}_{2.5}$ data of the ambient air quality in Hubei during February and March of 2016–2020 were obtained from the Department of Ecology Environment of Hubei Province [24], involving 12 prefecture-level cities, including Wuhan (WH), Yichang (YC), Jingzhou (JZ), Xiangyang (XY), Jingmen (JM), Shiyan (SY), Suizhou (SZ), Xiaogan (XG), Huangshi (HS), Huanggang (HG), Xianning (XN), and Ezhou (EZ) (Figure 1). Prefecture-level cities' air quality data are the average values of observed pollutants obtained from several state-controlled monitoring points within the jurisdiction. The meteorological data for the same period are the hourly resolution data in February and March of 2016–2020 at national

observation stations archived in the database of the National Meteorological Information Center (NMIC) of the China Meteorological Administration (CMA).

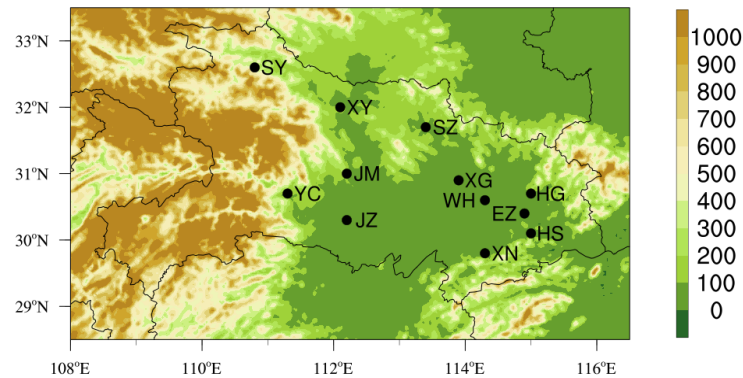


Figure 1. Terrain elevation (unit: m) and geographic locations of 12 prefectural cities in Hubei Province (WH: Wuhan; YC: Yichang; JM: Jingmen; SY: Shiyan; XY: Xiangyang; JZ: Jingzhou; SZ: Suizhou; XG: Xiaogan; HS: Huangshi; HG: Huanggang; EZ: Ezhou; XN: Xianning).

2.2. EOF Method

Empirical orthogonal function (EOF) [25] analysis is a method that is used to identify patterns of simultaneous variation [26,27]. It is also a method for dimensionality reduction analysis of spatial-temporal data, being widely used in the field of meteorology, mainly for the spatial-temporal distribution of meteorological elements. Depending on it, scientists can decompose the element fields of a large amount of observation data into the sum products of the time function and the space function so as to objectively and quantitatively reflect the changes in the element fields [28,29]. Its basic principle is to decompose the variable matrix X_{mn} composed of n times observations (sample time length) at m spatial points into a linear combination of the spatial eigenvector matrix V and the corresponding time coefficient matrix Z . In environmental data analysis, the eigenvector corresponds to the spatial sample, named spatial mode, and the principal component corresponds to the time change, called the time coefficient. In this study, we decompose the hourly $PM_{2.5}$ observation data of 12 cities into a linear combination of the spatial eigenvector matrix V and the corresponding time coefficient matrix Z , namely:

$$X_{mn} = \begin{bmatrix} v_{11} & \cdots & v_{1n} \\ \vdots & & \vdots \\ v_{m1} & \cdots & v_{mn} \end{bmatrix} \begin{bmatrix} z_{11} & \cdots & z_{1n} \\ \vdots & & \vdots \\ z_{m1} & \cdots & z_{mn} \end{bmatrix} \tag{1}$$

Use Fortran software to process X_{mn} as an anomaly, we get the eigen root λ_m and eigenvector v_m of the real symmetric matrix and then calculate the variance contribution rate ρ_i of the i -th eigenvector and the cumulative variance contribution rate P_i of the first p eigenvectors.

$$\rho_i = \lambda_i / \sum_{i=1}^m \lambda_i \tag{2}$$

$$P_i = \sum_{i=1}^p \lambda_i / \sum_{i=1}^m \lambda_i \tag{3}$$

The eigenvector represents the variability distribution structure of a regional climate variable field in a region, and its spatial distribution pattern represents the main distribution structure of the field; when the corresponding time coefficient is positive, it indicates the same variation trend between the temporal variable and this distribution pattern. Conversely, when the coefficient is negative, it indicates the contrary variation tendency

between the two, and the higher the value, the more significant the corresponding spatial distribution pattern [30].

To investigate the spatial-temporal characteristics of the PM_{2.5} mass concentration in Hubei Province during the COVID-19 pandemic, the hourly PM_{2.5} mass concentration anomalies in Hubei from February to March during five years (2016–2020) were decomposed by the EOF and the main spatial distribution characteristics of PM_{2.5} were extracted in this study.

2.3. Numerical Modeling

The Weather Research and Forecasting model coupled with Chemistry (WRF-Chem) has achieved the two-way coupling of atmospheric dynamics and chemistry, providing chemical models with online pollutant transport, dry and wet deposition, gas-phase chemistry, aerosol formation, radiation and photodecomposition rate, aerosol parameterization, and other chemical processes. It has been widely used in international studies of atmospheric environments [31–35]. The Central China Regional Numerical Prediction System of Environmental Meteorology, which is primarily based on the WRF-Chem model, has showed good performance in operational evaluation and application [36,37]. Based on this model system framework, a 27 km/9 km double-nested model has been designed, with d01 covering most parts of East Asia and d02 covering Central China. The physical parameterization schemes include the Yonsei University (YSU) [38] scheme for boundary layer, the rapid and accurate radiative transfer model (RRTM) [39] for long-wave radiation and the Goddard scheme for shortwave radiation [40], the Noah land surface model [41], the Regional Acid Deposition Model version 2 (RADM2) [42] for gas-phase chemistry, and the Modal Aerosol Dynamics Model for Europe/Secondary Organic Aerosol Model (MADE/SORGAM) for the aerosol chemical mechanism.

Anthropogenic emissions were taken from the Multi-resolution Emission Inventory for China [43] for the year 2016 [44], and the onset and end time dates of the control test (CT) simulation were designed to be 28 December 2019 and 29 February 2020, respectively. The 1 × 1 National Center for Environmental Prediction's (NCEP) Final Analysis (FNL) dataset [45] provided the meteorological initial and boundary conditions. The lateral boundary was updated every 6 h, model-nudging four-dimensional assimilation process was used to nudge the model outputs to the observations, and finally, the model spin-up time was eliminated. On this basis, the emission sources in Hubei Province were closed for a sensitivity test (ST), and the result could be approximated as the impact of external source transmission on pollution changes in Hubei, regardless of the nonlinear error of the chemical reaction.

3. Results

3.1. PM_{2.5} Concentration Variation in Hubei during COVID-19

Hubei witnessed a downward trend of its average PM_{2.5} concentration from February to March of 2016–2019 (Figure 2a). Based on this linear trend, the expected PM_{2.5} annual concentration in 2020 was 51 µg/m³, 11 µg/m³ (21%) higher than the actual value of 40 µg/m³. This phenomenon reflects the impact extent of emission reduction during the COVID-19 pandemic on the PM_{2.5} concentration in Hubei Province, that is, the less human activities during the period might contribute to the 11 µg/m³ (21%) drop in the PM_{2.5} concentration in Hubei Province.

Figure 2b,c shows the spatial differences of the PM_{2.5} concentrations in the major cities of Hubei Province and the provincial average PM_{2.5} concentration from February to March during 2016–2019 relative to the pollution situation in the same period in 2020. As shown in the figure, positive anomalies were observed in WH, EZ, XY, JM, JZ, and YC in 2016–2019 (Figure 2b), i.e., there were two high PM_{2.5} concentration centers located in the urban circle of WH and the pollution transport channel cities in central-western Hubei, respectively [46]. In 2020, negative anomalies were observed in WH, EZ, and JZ due to COVID-19, while positive anomalies were found in XY, JM, and YC, of which the anomaly

in JM significantly increased (Figure 2c). This means that in the COVID-19 low-emission scenario (LES), the high $PM_{2.5}$ concentration center at the urban circle of WH disappeared, while another high-value center of $PM_{2.5}$ remained in the cities of XY, JM, and YC along the transport channel in central-western Hubei.

Given that the changes in the air pollutant concentration were simultaneously affected by emission sources, meteorological conditions, and geographical factors, the $PM_{2.5}$ concentration centers in those regions with a high $PM_{2.5}$ concentration normally contributed by local emission sources weakened considerably in the LES during COVID-19. In contrast, those areas affected more by meteorological and geographic conditions (e.g., areas under the effect of regional pollutant transport and accumulated pollutants in front of mountains) had higher values of the $PM_{2.5}$ concentration during the same period. For Hubei Province, the disappearance of high-value $PM_{2.5}$ centers in the WH urban circle and the prominent performance characteristics of high-value $PM_{2.5}$ centers in the transport channel cities in central-western Hubei in the LES are to be further discussed below, during which the EOF spatial-temporal decomposition will be conducted of the Hubei $PM_{2.5}$ concentration anomalies for the periods of February to March in 2016–2019 and in 2020.

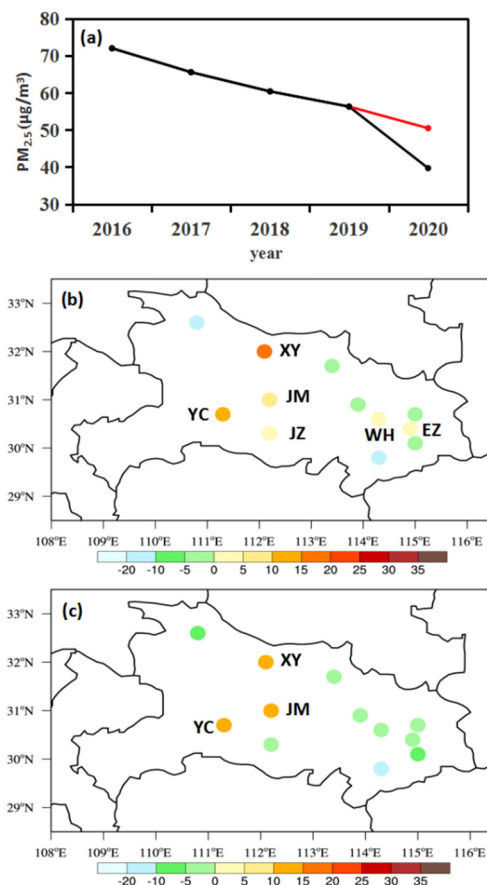


Figure 2. Changes in particulate matter smaller than $2.5 \mu m$ ($PM_{2.5}$) during the coronavirus disease 2019 (COVID-19) outbreak in Hubei Province. (a) The February–March average concentration (black dot) during 2016–2020 (the red dot represents the value for 2020 calculated based on the 2016–2019 linear fitting trend), (b) spatial anomaly of the average $PM_{2.5}$ concentration in Hubei Province from February to March in 2016–2019, and (c) spatial anomaly of average the $PM_{2.5}$ concentration in Hubei Province during the COVID-19 pandemic.

3.2. Spatial-Temporal Variation Characteristics of $PM_{2.5}$ Pollution in Hubei Based on EOF Decomposition

The annual statistics of hourly $PM_{2.5}$ mass concentration anomalies from February to March 2016–2020 in 12 prefectural cities in Hubei was analyzed via the EOF. Table 1 gives

the variance contributions of time coefficients of the first two eigenvectors. The variance contributions of the first eigenvector in each year of 2016–2020 were at 64%, 64%, 62%, 66%, and 69% respectively, and the variance contributions of the second one were 13%, 14%, 15%, 15%, and 11%, respectively. The accumulated variance contributions of the first two eigenvectors almost reach about 80%, which can reflect the main characteristics of the spatial-temporal distribution of the PM_{2.5} mass concentration in Hubei Province. The EOF decomposition can extract the relatively stable annual eigenvectors of the main modes. By comparing the first two main modes from February to March in 2020 and the same period in 2016–2019, we disclosed the spatial-temporal variation characteristics of PM_{2.5} in Hubei in the LES during COVID-19.

Table 1. Variance contribution of the first two eigenvectors of PM_{2.5} empirical orthogonal function (EOF) decomposition in Hubei Province.

Eigenvectors/Year	2016	2017	2018	2019	2020
EOF1	64.09	64.01	61.57	65.69	68.95
EOF2	13.43	13.93	14.94	14.78	10.65
EOF1 + EOF2	77.52	77.94	76.51	80.47	79.60

3.2.1. Diurnal Variation Characteristics of PM_{2.5} in Hubei

The hourly averages from 00:00 to 23:00 local time (LC, UTC +8) calculated based on the first mode time coefficient in 2016–2020 were used to characterize the daily variation of PM_{2.5} in Hubei. Figure 3 shows the daily variation of the first mode time coefficient. As shown in the figure, the daily variation trend is in line with the double-ridges-and-one-trough pattern. The corresponding first mode is the pollution distribution across the whole province (Figure 4a,c). When the daily variation is positive at 20:00–12:00 LC, it indicates a positive anomaly of the PM_{2.5} concentration in Hubei, and when it is negative at 12:00–20:00 LC, it means a negative anomaly.

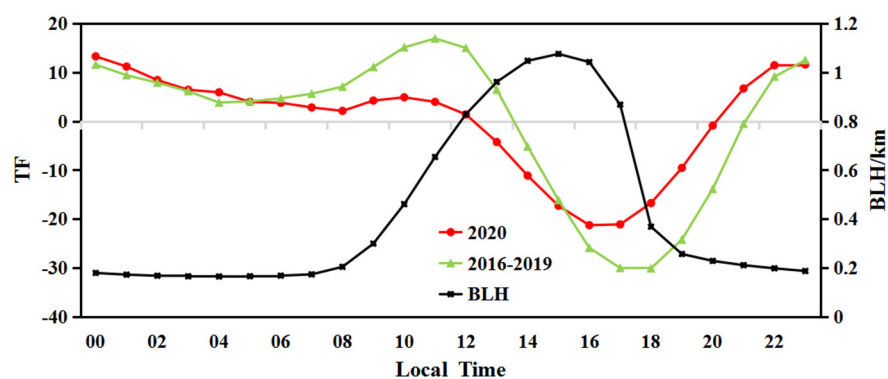


Figure 3. Diurnal variations of the first mode time factor of PM_{2.5} EOF decomposition and the boundary layer height in Hubei Province. (The black line is the boundary layer height curve, the green dotted line is the daily change in the first mode time coefficient from 2016 to 2019, and the red dotted line is the daily change of the first mode time coefficient in 2020).

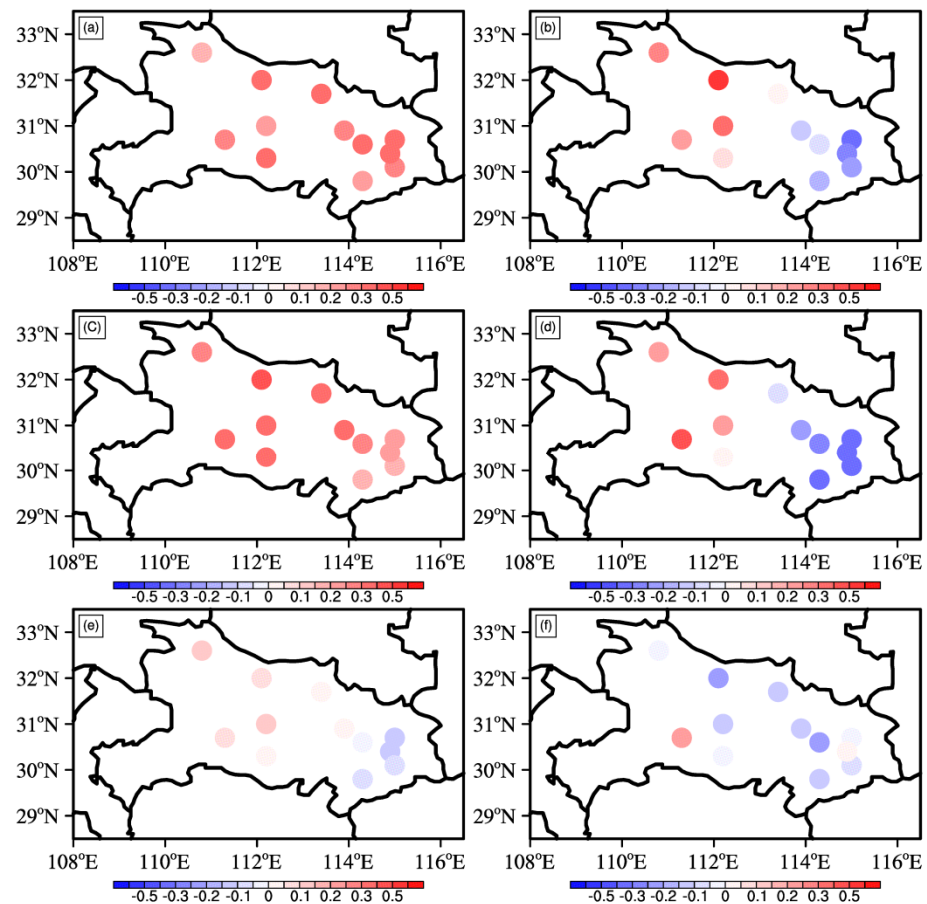


Figure 4. Spatial distribution of eigenvectors of $PM_{2.5}$ mass concentration EOF decomposition in Hubei Province. (a) Average of 2016–2019 EOF1, (b) average of 2016–2019 EOF2, (c) 2020 EOF1, (d) 2020 EOF2, (e) difference between 2020 and 2016–2019 EOF1, and (f) difference between 2020 and 2016–2019 EOF2.

By comparing the variation characteristics of daily $PM_{2.5}$ in 2016–2019 and 2020, we found that the daytime peak eigenvalue at 08:00–12:00 LC during the 2020 pandemic declined significantly, but the nighttime peak value did not change much, which indicates that the former is dominated by human-induced emission, while the latter is controlled by meteorological conditions. Accordingly, from the view of emission control, human activities are a major contributor to the $PM_{2.5}$ peak value at 08:00–12:00 LC. So, the daytime $PM_{2.5}$ pollution peak can be effectively reduced by staggering emission control and weakening the impact of human activities within this time period. Given adverse meteorological conditions at night, the nighttime pollution peak in the LES during COVID-19 was more prominent, and its eigenvalue was even higher than that in the daytime, denoting a more significant impact of meteorological conditions on $PM_{2.5}$ pollution changes in the LES. Therefore, when more rigorous emission regulations are to be implemented, the control of night pollution emissions cannot be ignored in order to gradually reduce night pollution peaks.

Combined with the daily variation of the atmospheric boundary layer height (BLH) (5-year average from 2016 to 2020), it can be seen that the atmospheric diffusion conditions are the best in the daytime and the corresponding daily variation in $PM_{2.5}$ is the maximum negative anomaly. During the 2020 pandemic, the occurrence time of the maximum negative anomaly in Hubei was more consistent with the BLH daily variation, which was 1–2 h earlier than that in 2016–2019. This indicates that the $PM_{2.5}$ concentration in the LES is more sensitive to the BLH change, i.e., the impact of meteorological conditions on $PM_{2.5}$ pollution variation is more noticeable in the LES.

3.2.2. Spatial Variation Characteristics of PM_{2.5} in Hubei

Figure 4 shows the 4-year average (2016–2019) of the first and second modes of the PM_{2.5} concentration anomaly decomposition and the spatial vector distribution in 2020 in Hubei. The spatial vector values of the first mode in each year are all greater than 0 (Figure 4a,c), showing the characteristics of consistent PM_{2.5} mass concentration variation in Hubei. When the corresponding time coefficient is greater than 0, the PM_{2.5} mass concentration in Hubei is generally high, representing the characteristics of pollution distribution in Hubei as a whole; when the time coefficient is less than 0, the PM_{2.5} mass concentration in Hubei is low. The spatial distribution of the mean difference in the spatial vector values of the first mode between 2020 and 2016–2019 is displayed in Figure 4e. As seen from the figure, the difference value is negative in the eastern part and positive in the western part of Hubei, which indicates that changes occurred in the PM_{2.5} pollution variability structure of the first mode, with an increase in the western part and a decrease in the eastern part.

The spatial vector values of the second mode in each year show an opposite variation of PM_{2.5} variability in the eastern and western parts of Hubei (Figure 4b,d). When the corresponding time coefficient is greater than 0, it means a positive PM_{2.5} concentration anomaly in the western part but a negative anomaly in the eastern part; when the time coefficient is less than 0, the situation is reversed. Figure 4f reveals the spatial distribution of the average difference of the second mode spatial vector values between the year 2020 and 2016–2019. The difference value of the mode spatial vector fields between the two is relatively positive in YC, which suggests that the variability of PM_{2.5} pollution in most parts of the province reduced due to the emission reduction during the epidemic, except the increased PM_{2.5} pollution variability in YC. YC is located in the transition zone from Wuling Mountains and Qinba Mountains in western Hubei to the Jiangnan Plain, surrounded by mountains on three sides, with the southwest as a plain (Figure 1). Such terrain is very favorable for the transport of pollutants. During the COVID-19 pandemic in Hubei, the local calm weather (0–2 m/s) and short-distance southeast wind transport (2–4 m/s southwest wind, Figure S1) caused the pollution in YC. In other words, the PM_{2.5} pollution variability increased in the YC region due to the meteorological conditions and the stacking effect caused by the terrain.

3.3. Variation Characteristics of Inter-Regional Transport

Figure 5 presents the distribution of the PM_{2.5} concentration anomaly in WH varying with the local wind speed and direction in the case of a positive time series (i.e., high values of PM_{2.5} concentration over the whole province) in 2016–2019 and 2020. In the past years, WH had scattered high-value centers of the PM_{2.5} concentration anomaly (Figure 5a). The PM_{2.5} pollution might be caused by not only calm weather but also the pollutants conveyed by winds from different directions, of which the major pollution was generated by the long-distance inter-regional transport of pollutants along with northerly and northeasterly winds. This result is consistent with the conclusion by Yu et al. (2020) [22]. However, during the COVID-19 pandemic, the high-value center of the WH PM_{2.5} concentration anomaly (Figure 5b) was mainly concentrated in the area affected by the east-to-northeast wind at a speed of 2–4 m/s, without any pollution resulting from the locally static and steady accumulation (0–2 m/s wind speed) and long-distance inter-regional transport (greater than 4 m/s wind speed).

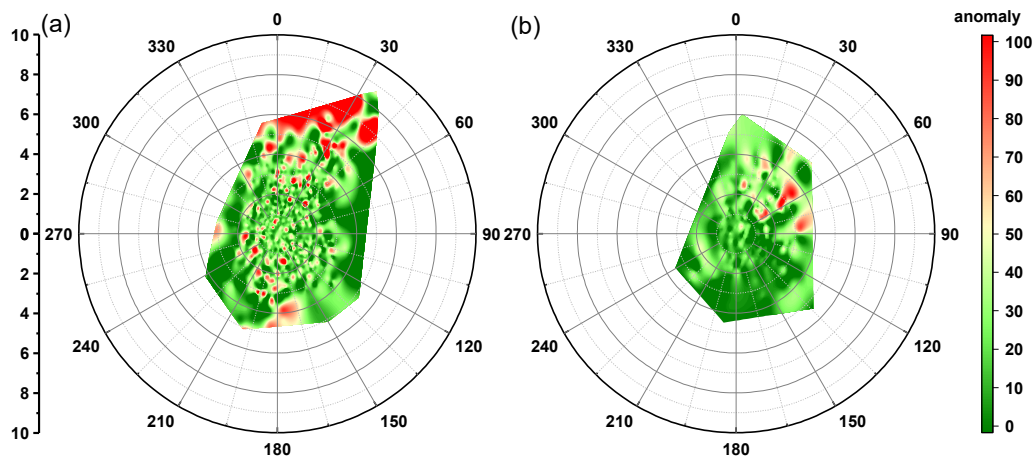


Figure 5. Polar plots of hourly variations in wind speed (round radius, unit: m/s) and direction (angles) to the surface $PM_{2.5}$ concentration anomaly (color contours, unit: $\mu g/m^3$) of the first eigenvectors. (a) WH in 2016–2019 and (b) WH in 2020.

Based on the empirical relationship between wind speed and $PM_{2.5}$ pollution in different weather patterns, a wind speed of 0–2 m/s represents calm weather, a wind speed of ≥ 4 m/s indicates $PM_{2.5}$ long-distance inter-regional transport, and a wind speed of 2–4 m/s indicates short-distance transport within the urban clusters [22,47,48]. Figure 6 shows the declined percentage of $PM_{2.5}$ anomalies at different wind speeds during the COVID-19 pandemic relative to that during 2016–2019. WH and JM are, respectively, typical cities of the urban circle in the eastern part and the central western pollution transport channels in Hubei Province. It can be seen from the figure that when the wind speed in WH (JM) is 0–2 m/s and 2–4 m/s, the $PM_{2.5}$ pollution concentration anomaly decreases by 52% (18%) and 16% (9.1%), respectively; when the wind speed is ≥ 4 m/s, the $PM_{2.5}$ pollution anomaly decreases by 47% in WH but increases by 8.8% in JM. This means that during the epidemic period, the $PM_{2.5}$ concentration greatly reduced in WH due to the less accumulation of local-sourced and long-distance inter-regional transport of pollutants [49], but the short-distance transport of $PM_{2.5}$ was the major pollution in the urban circle. In the JM area, however, the local accumulation of $PM_{2.5}$ and the short-distance transport of pollutants weakened to some extent during the pandemic, and the long-distance inter-regional transport of $PM_{2.5}$ concentration anomaly increased.

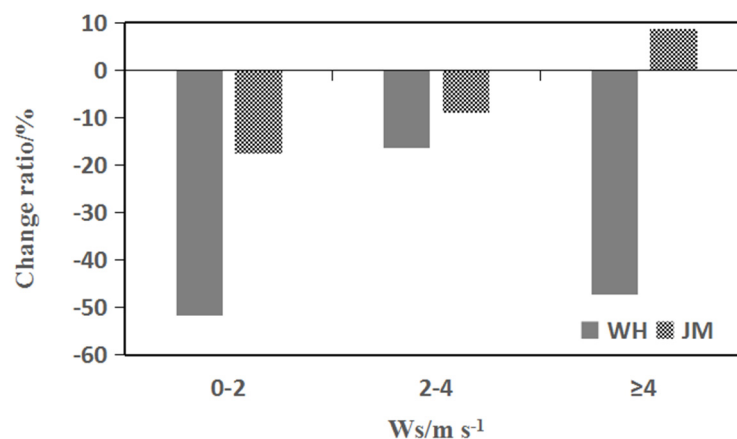


Figure 6. The percentage reduction in the $PM_{2.5}$ concentration anomaly of the first eigenvectors in WH and JM under different wind speed conditions during the COVID-19 pandemic.

In general, WH had a much lower $PM_{2.5}$ concentration anomaly than JM during the COVID-19 pandemic. In eastern Hubei, $PM_{2.5}$ pollution significantly lessened via the

control measures of local emission sources and long-distance inter-regional transport of pollutants, while the central-western part of Hubei still observed large-value centers of the $PM_{2.5}$ concentration, which was the contribution from the long-distance inter-regional transport of pollutants.

Based on comparison of the average $PM_{2.5}$ concentration simulated by the WRF-Chem control test (CT) and the observations during 1–29 February 2020 (Figure 7a), we can see the simulation result can basically reflect the actual $PM_{2.5}$ concentration in the prefectural cities of Hubei Province. Figure 7b shows the sensitivity test (ST) used to simulate the concentration of $PM_{2.5}$ pollution in Hubei from external sources during COVID-19. We found in the figure that the $PM_{2.5}$ concentration in the pollution transport channel from XY through JM to YC was significantly higher than that in the eastern part, which denotes that inter-regional transport of air pollutants intensified $PM_{2.5}$ pollution in central-western Hubei. This further shows that during the epidemic period, regional transmission of pollutants aggravated the $PM_{2.5}$ changes in the pollution transport channel cities in the central-western region of Hubei, causing the XY–JM–YC region to remain the high-value center of the $PM_{2.5}$ concentration during the epidemic.

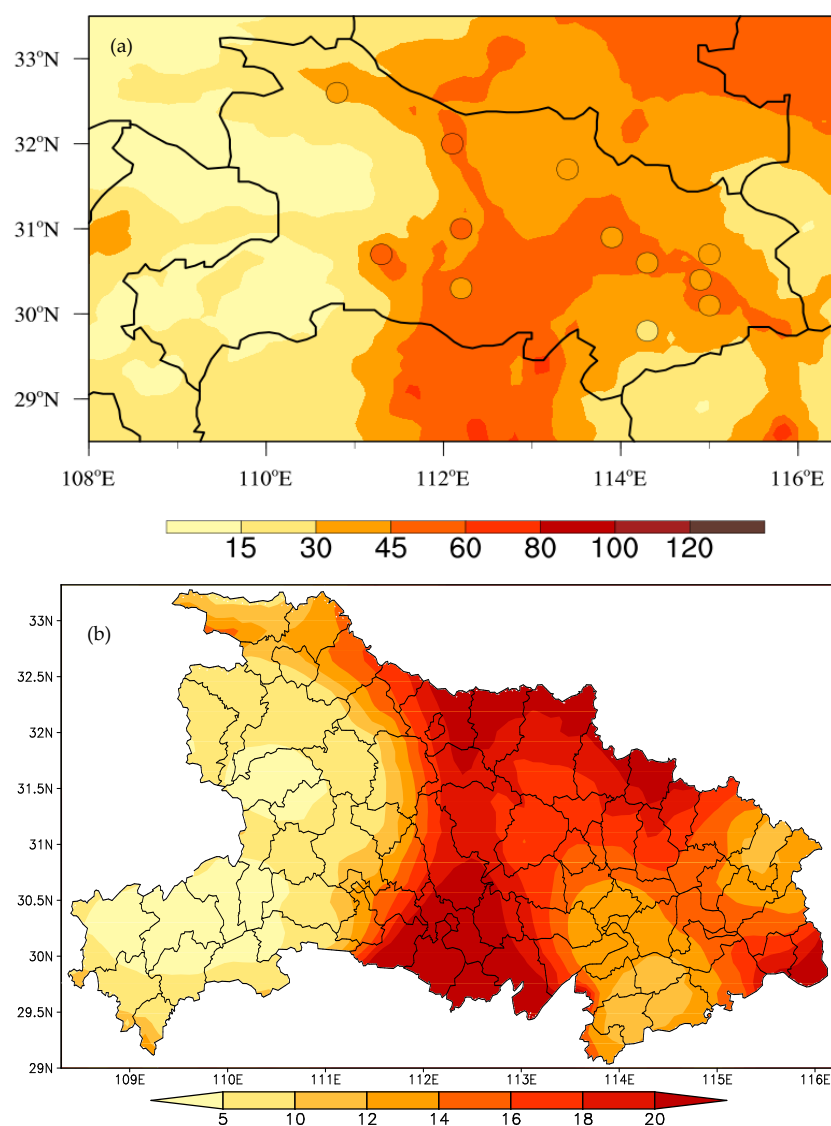


Figure 7. (a) Average $PM_{2.5}$ concentration (unit: $\mu\text{g}/\text{m}^3$) in February 2020 simulated by the Weather Research and Forecasting Model coupled with Chemistry (WRF-Chem) control test (CT, shaded) and observations (dotted) in cities in Hubei; (b) concentration (unit: $\mu\text{g}/\text{m}^3$) of $PM_{2.5}$ pollution in Hubei from external sources simulated by a sensitivity test (ST).

4. Discussion and Conclusions

In 2020, when COVID-19 broke out as a global pandemic, WH went into lockdown on 23 January, followed by all the other cities of Hubei Province. From February to March 2020, human activities in Hubei greatly decreased, leading to the low-level emission of pollutants and decreasing the average $PM_{2.5}$ concentration down to $40 \mu\text{g}/\text{m}^3$, 21% lower than expected. During the pandemic, the spatial distribution of $PM_{2.5}$ pollution varied greatly. The high-value center of the $PM_{2.5}$ concentration in the WH urban circle disappeared, but persisted in the pollution transport channel cities in the central-western part of Hubei Province.

EOF analysis, based on the $PM_{2.5}$ concentration anomaly from February to March in 2020 and the same period in 2016–2019, has shown that the $PM_{2.5}$ anomaly increased in the transport channel cities in central-western Hubei but decreased in the urban circle of WH in eastern Hubei. Under the influence of emission source control during COVID-19, eastern Hubei saw a great decrease in locally sourced $PM_{2.5}$ accumulation and long-distance inter-regional transport, while central-western Hubei experienced an increase in $PM_{2.5}$ long-distance inter-regional transport. Hu et al. (2020) [50] revealed that the regional $PM_{2.5}$ transport of Central-East China made large contributions to Hubei's heavy air pollution, and such contribution was greater in the western region than in the eastern region. Thus, it can be seen that the $PM_{2.5}$ high-value center in the urban circle of WH was dominated by high-level local emissions, while the high-value center in the transport channel cities in central-western Hubei was more affected by inter-regional transport. Though the emissions from the local pollution sources were greatly reduced during the COVID-19 pandemic, the contributions of meteorological and geographic conditions [51] were still there, so the inter-regional transport of pollutants kept the role of aggravating the $PM_{2.5}$ concentration in the central-western part of Hubei, leading to a prominent $PM_{2.5}$ high-value center.

During COVID-19, the 08:00–12:00 LC daytime peak eigenvalue of the $PM_{2.5}$ daily variation in Hubei Province decreased greatly, while the peak value at night was more prominent. This is very consistent with the daily variation of the BLH, indicating that the $PM_{2.5}$ concentration in the COVID-19 low-emission scenario was more sensitive to a BLH change. In other words, the meteorological conditions have a more obvious effect on the variation of $PM_{2.5}$ pollution in a low-emission scenario; this result is consistent with the conclusion by Shen et al. (2020) [6]. Accordingly, we can see that human activity is a very important factor for the peak value of $PM_{2.5}$ pollution from 08:00 to 12:00 LC. The daytime $PM_{2.5}$ pollution peak can be effectively reduced by regulating the emission to weaken the impact of human activities during this period of time. On the other hand, the control of the night pollution emissions should be strengthened so as to decrease the nighttime pollution peaks gradually.

Supplementary Materials: <https://www.mdpi.com/2073-4433/12/2/250/s1>. Figure S1: A polar plot of the hourly variations in wind speed (round radius, in m/s) and direction (angles) to surface $PM_{2.5}$ concentration anomaly (color contours, in $\mu\text{g}/\text{m}^3$) of second eigenvector of YC in 2020.

Author Contributions: Conceptualization, Y.B. and T.Z.; Data curation, W.H.; Formal analysis, J.X.; Investigation, J.X.; Resources, S.K.; Visualization, J.X.; Writing—original draft, J.X.; Writing—review and editing, Y.B., T.Z. and S.K. All authors have read and agreed to the published version of the manuscript.

Funding: This research has been supported by the National Natural Science Foundation of China (grant nos. 41830965 and 42075186).

Data Availability Statement: The data used in this paper can be provided by Jie Xiong (xiongjie8707@sina.com) upon request.

Acknowledgments: This study was jointly funded by the National Natural Science Foundation of China (grant nos. 41830965 and 42075186).

Conflicts of Interest: The authors declare no conflict of interest.

References

1. Huang, X.; Ding, A.; Gao, J.; Zheng, B.; Zhou, D.; Qi, X.; Tang, R.; Wang, J.; Ren, C.; Nie, W.; et al. Enhanced secondary pollution offset reduction of primary emissions during COVID-19 lockdown in China. *Natl. Sci. Rev.* **2020**. [CrossRef]
2. Kong, S.F.; Li, L.; Li, X.X.; Yin, Y.; Chen, K.; Liu, D.; Yuan, L.; Zhang, Y.J.; Shan, Y.P.; Ji, Y.Q. The impacts of firework burning at the Chinese Spring Festival on air quality: Insights of tracers, source evolution and aging processes. *Atmos. Chem. Phys. Discuss.* **2015**, *15*, 2167–2184. [CrossRef]
3. Zheng, H.; Kong, S.; Chen, N.; Yan, Y.; Liu, D.; Zhu, B.; Xu, K.; Cao, W.; Ding, Q.; Lan, B.; et al. Significant changes in the chemical compositions and sources of PM_{2.5} in Wuhan since the city lockdown as COVID-19. *Sci. Total. Environ.* **2020**, *739*, 140000. [CrossRef]
4. Le, T.; Wang, Y.; Liu, L.; Yang, J.; Yung, Y.L.; Li, G.; Seinfeld, J.H. Unexpected air pollution with marked emission reductions during the COVID-19 outbreak in China. *Science* **2020**, *369*, 702–706. [CrossRef]
5. Wang, P.; Chen, K.; Zhu, S.; Wang, P.; Zhang, H. Severe air pollution events not avoided by reduced anthropogenic activities during COVID-19 outbreak. *Resour. Conserv. Recycl.* **2020**, *158*, 104814. [CrossRef] [PubMed]
6. Shen, L.; Zhao, T.; Wang, H.; Liu, J.; Bai, Y.; Kong, S.; Zheng, H.; Zhu, Y.; Shu, Z. Importance of meteorology in air pollution events during the city lockdown for COVID-19 in Hubei Province, Central China. *Sci. Total. Environ.* **2021**, *754*, 142227. [CrossRef]
7. Bauwens, M.; Compennolle, S.; Stavrou, T.; Müller, J.; Van Gent, J.; Eskes, H.; Levelt, P.F.; Van Der, A.R.; Veefkind, J.P.; Vlietinck, J.; et al. Impact of coronavirus outbreak on NO₂ pollution assessed using TROPOMI and OMI observations. *Geophys. Res. Lett.* **2020**, *47*, e2020GL087978. [CrossRef]
8. Zhang, R.; Zhang, Y.; Lin, H.; Feng, X.; Fu, T.-M.; Wang, Y. NO_x emission reduction and recovery during COVID-19 in East China. *Atmosphere* **2020**, *11*, 433. [CrossRef]
9. Cui, Y.; Ji, D.; Maenhaut, W.; Gao, W.; Zhang, R.; Wang, Y. Levels and sources of hourly PM_{2.5}-related elements during the control period of the COVID-19 pandemic at a rural site Beijing and Tianjin. *Sci. Total. Environ.* **2020**, *744*, 140840. [CrossRef] [PubMed]
10. Yuan, Q.; Qi, B.; Hu, D.; Wang, J.; Zhang, J.; Yang, H.; Zhang, S.; Liu, L.; Xu, L.; Li, W. Spatiotemporal variations and reduction of air pollutants during the COVID-19 pandemic in a megacity of Yangtze River Delta in China. *Sci. Total. Environ.* **2021**, *751*, 141820. [CrossRef]
11. Xu, L.; Zhang, J.; Sun, X.; Xu, S.; Shan, M.; Yuan, Q.; Liu, L.; Du, Z.; Liu, D.; Xu, D.; et al. Variation in concentration and sources of black carbon in a megacity of China during the COVID-19 pandemic. *Geophys. Res. Lett.* **2020**, *47*, e2020GL090444. [CrossRef]
12. Kim, C.-H.; Park, S.-Y.; Kim, Y.-J.; Chang, L.-S.; Song, S.-K.; Moon, Y.-S.; Song, C.-K. A numerical study on indicators of long-range transport potential for anthropogenic particulate matters over northeast Asia. *Atmos. Environ.* **2012**, *58*, 35–44. [CrossRef]
13. Lang, J.; Cheng, S.; Li, J.; Chen, D.; Zhou, Y.; Wei, X.; Han, L.; Wang, H. A monitoring and modeling study to investigate regional transport and characteristics of PM_{2.5} pollution. *Aerosol Air Qual. Res.* **2013**, *13*, 943–956. [CrossRef]
14. Wu, D.; Fung, J.C.H.; Yao, T.; Lau, A.K.H. A study of control policy in the Pearl River Delta region by using the particulate matter source apportionment method. *Atmos. Environ.* **2013**, *76*, 147. [CrossRef]
15. Xu, X.D.; Ding, G.A. Generalized method of urban air pollutant source tracking and integration approach of nudging source assimilation. *Eng. Sci.* **2012**, *14*, 10–22. (In Chinese)
16. Yang, Y.; Quan, J.; Wang, Y.; Zhang, Y.; Cao, G.; Zhang, Q.; Wang, W.; Wang, J.; Sun, J.; Zhang, X.; et al. Factors contributing to haze and fog in China. *Chin. Sci. Bull. (ChinVer)* **2013**, *58*, 1178–1187. [CrossRef]
17. Gao, M.; Carmichael, G.R.; Wang, Y.; Saide, P.E.; Yu, M.; Xin, J.; Liu, Z.; Wang, Z. Modeling study of the 2010 regional haze event in the North China Plain. *Atmos. Chem. Phys.* **2016**, *16*, 1673–1691. [CrossRef]
18. Li, J.; Du, H.; Wang, Z.; Sun, Y.; Yang, W.; Li, J.; Tang, X.; Fu, P. Rapid formation of a severe regional winter haze episode over a mega-city cluster on the North China Plain. *Environ. Pollut.* **2017**, *223*, 605–615. [CrossRef]
19. Wu, P.; Ding, Y.; Liu, Y. Atmospheric circulation and dynamic mechanism for persistent haze events in the Beijing-Tianjin-Hebei region. *Adv. Atmos. Sci.* **2017**, *34*, 429–440. [CrossRef]
20. Ji, Y.; Qin, X.; Wang, B.; Xu, J.; Shen, J.; Chen, J.; Huang, K.; Deng, C.; Yan, R.; Xu, K.; et al. Counteractive effects of regional transport and emission control on the formation of fine particles: A case study during the Hangzhou G20 summit. *Atmos. Chem. Phys.* **2018**, *18*, 13581–13600. [CrossRef]
21. Shen, L.-J.; Wang, H.-L.; Zhao, T.; Liu, J.; Bai, Y.; Kong, S.-F.; Shu, Z.-Z. Characterizing regional aerosol pollution in central China based on 19 years of MODIS data: Spatiotemporal variation and aerosol type discrimination. *Environ. Pollut.* **2020**, *263*, 114556. [CrossRef]
22. Yu, C.; Zhao, T.; Bai, Y.; Zhang, L.; Kong, S.; Yu, X.; He, J.; Cui, C.; Yang, J.; You, Y.; et al. Heavy air pollution with a unique “non-stagnant” atmospheric boundary layer in the Yangtze River middle basin aggravated by regional transport of PM_{2.5} over China. *Atmos. Chem. Phys.* **2020**, *20*, 7217–7230. [CrossRef]
23. Lu, M.; Tang, X.; Wang, Z.; Wu, L.; Chen, X.; Liang, S.; Zhou, H.; Wu, H.; Hu, K.; Shen, L.; et al. Investigating the Transport Mechanism of PM_{2.5} Pollution during January 2014 in Wuhan, Central China. *Adv. Atmos. Sci.* **2019**, *36*, 1217–1234. [CrossRef]
24. Department of Ecology and Environment Hubei Province. Available online: <http://sthjt.hubei.gov.cn/hjsj/sjfb/> (accessed on 12 January 2021).
25. Lorenz, E.N. *Empirical Orthogonal Functions and Statistical Weather Prediction*; Statistical Forecasting Project; Scientific Report No. 1; Dep. Meteorol MIT: Cambridge, MA, USA, 1956; p. 49.

26. von Storch, H.; Zwiers, F.W. *Statistical Analysis in Climate Research*; Cambridge University Press: Cambridge, UK, 2002; p. 496.
27. Schepanski, K.; Mallet, M.; Heinold, B.; Ulrich, M. North African dust transport toward the western Mediterranean basin: Atmospheric controls on dust source activation and transport pathways during during June–July 2013. *Atmos. Chem. Phys.* **2016**, *16*, 14147–14168. [[CrossRef](#)]
28. Wu, X.Y.; Ye, C.Z.; Wang, Q. Analysis on the climatic characteristics of precipitation in rainy season in the Two-lake Region. *Torrential Rain Disasters* **2016**, *35*, 497–503. (In Chinese)
29. Sun, Y.; Yin, D.P.; Yao, L.N.; Cao, S.Y. Spatial-temporal distribution and circulation features of the Meiyu precipitation anomaly in Jiangsu in the latest 50 years. *Torrential Rain Disasters* **2012**, *31*, 149–154. (In Chinese)
30. Wei, F.Y. *Modern Climate Statistical Diagnosis and Prediction Technology: II*; China Meteorological Press: Beijing, China, 2007. (In Chinese)
31. Sha, T.; Ma, X.; Wang, J.; Tian, R.; Zhao, J.; Cao, F.; Zhang, Y.-L. Improvement of inorganic aerosol component in PM_{2.5} by constraining aqueous-phase formation of sulfate in cloud with satellite retrievals: WRF-Chem simulations. *Atmos. Chem. Phys.* **2020**. in review. [[CrossRef](#)]
32. Grell, G.A.; Peckham, S.E.; Schmitz, R.; McKeen, S.A.; Frost, G.; Skamarock, W.C.; Edere, B. Fully coupled “online” chemistry within the WRF model. *Atmos. Environ.* **2005**, *39*, 6957–6975. [[CrossRef](#)]
33. Gustafson, W.I.; Chapman, E.G.; Ghan, S.J.; Easter, R.C.; Fast, J.D. Impact on modeled cloud characteristics due to simplified treatment of uniform cloud condensation nuclei during NEAQS 2004. *Geophys. Res. Lett.* **2007**, *34*, 255–268. [[CrossRef](#)]
34. Guo, J.; He, J.; Liu, H.; Miao, Y.; Liu, H.; Zhai, P. Impact of various emission control schemes on air quality using WRF-Chem during APEC China 2014. *Atmos. Environ.* **2016**, *140*, 311–319. [[CrossRef](#)]
35. Lennartson, E.M.; Wang, J.; Gu, J.; Garcia, L.C.; Ge, C.; Gao, M.; Choi, M.; Saide, P.; Carmichael, G.R.; Kim, J.; et al. Diurnal variation of aerosol optical depth and PM_{2.5} in South Korea: A synthesis from AERONET, satellite (GOCI), KORUS-AQ observation, and the WRF-Chem model. *Atmos. Chem. Phys.* **2018**, *18*, 15125–15144. [[CrossRef](#)]
36. Bai, Y.; Qi, H.; Zhao, T.; Zhou, Y.; Liu, L.; Xiong, J.; Zhou, Z.; Cui, C. Simulation of the responses of rainstorm in the Yangtze River Middle Reaches to changes in anthropogenic aerosol emissions. *Atmos. Environ.* **2020**, *220*, 117081. [[CrossRef](#)]
37. Liu, L.; Bai, Y.Q.; Lin, C.Z.; Yang, H. Evaluation of Regional Air Quality Numerical Forecasting System in Central China and Its Application for Aerosol Radiative Effect. *Meteorol. Mon.* **2018**, *44*, 1179–1190. (In Chinese)
38. Hong, S.Y.; Noh, Y.; Dudhia, J. A New Vertical Diffusion Package with an Explicit Treatment of Entrainment Processes. *Mon. Weather Rev.* **2006**, *134*, 2318–2341. [[CrossRef](#)]
39. Mlawer, E.J.; Taubman, S.J.; Brown, P.D.; Iacono, M.J.; Clough, S.A. Radiative transfer for inhomogeneous atmospheres: RRTM, a validated correlated-k model for the longwave. *J. Geophys. Res.* **1997**, *102*, 16663. [[CrossRef](#)]
40. Chou, M.D.; Suarez, M.J. *An Efficient Thermal Infrared Radiation Parameterization 491 for Use in General Circulation Models*; NASA Technical Memorandum 104606; National Aeronautics and Space Administration: Greenbelt, MD, USA, 1994; p. 85.
41. Tewari, M.; Chen, F.; Wang, W.; Dudhia, J.; LeMone, M.A.; Mitchell, K.; Gayno, E.K.; Wegiel, G.J.; Cuenca, R.H. Implementation and verification of the unified Noah land surface model in the WRF model. In Proceedings of the 20th conference on weather analysis and forecasting/16th conference on numerical weather prediction, Seattle, WA, USA, 12–16 January 2004; pp. 11–15.
42. Stockwell, W.R.; Middleton, P.; Chang, J.S.; Tang, X. The second generation regional acid deposition model chemical mechanism for regional air quality modeling. *J. Geophys. Res. Atmos.* **1990**, *95*, 16343–16367. [[CrossRef](#)]
43. MEIC Model. Available online: <http://www.neicmodel.org> (accessed on 12 January 2021).
44. Li, M.; Zhang, Q.; Kurokawa, J.-I.; Woo, J.-H.; He, K.; Lu, Z.; Ohara, T.; Song, Y.; Streets, D.G.; Carmichael, G.R.; et al. MIX: A mosaic Asian anthropogenic emission inventory under the international collaboration framework of the MICS-Asia and HTAP. *Atmos. Chem. Phys.* **2017**, *17*, 935–963. [[CrossRef](#)]
45. NCEP FNL Operational Model Global Tropospheric Analyses, continuing from July 1999. Available online: <http://rda.ucar.edu/datasets/ds083.2/> (accessed on 12 January 2021).
46. Qi, H.X.; Cui, C.G.; Zhao, T.L.; Bai, Y.Q.; Liu, L. Numerical simulation on the characteristics of PM_{2.5} heavy pollution and the influence of weather system in Hubei Province in winter 2015. *Meteor Mon.* **2019**, *45*, 1113–1122. (In Chinese)
47. Lu, M.; Tang, X.; Wang, Z.; Gbaguidi, A.; Liang, S.; Hu, K.; Wu, L.; Wu, H.; Huang, H.; Shen, L. Source tagging modeling study of heavy haze episodes under complex regional transport processes over Wuhan megacity, Central China. *Environ. Pollut.* **2017**, *231*, 612–621. [[CrossRef](#)] [[PubMed](#)]
48. Yue, Y.Y.; Wang, X.L.; Zhang, M.X.; Cao, W.X.; Zhou, Y.; Chen, S.N.; Zhu, Y. Air quality condition in Wuhan and its relationship to meteorological factors. *Torrential Rain Disasters* **2016**, *35*, 271–278. (In Chinese)
49. Lian, X.; Huang, J.; Huang, R.; Liu, C.; Wang, L.; Zhang, T. Impact of city lockdown on the air quality of COVID-19-hit of Wuhan city. *Sci. Total. Environ.* **2020**, *742*, 140556. [[CrossRef](#)] [[PubMed](#)]
50. Hu, W.; Zhao, T.; Bai, Y.; Kong, S.; Xiong, J.; Sun, X.; Yang, Q.; Gu, Y.; Lu, H. Importance of regional PM_{2.5} transport and precipitation washout in heavy air pollution in the Twain-Hu Basin over Central China: Observational analysis and WRF-Chem simulation. *Sci. Total. Environ.* **2021**, *758*, 143710. [[CrossRef](#)] [[PubMed](#)]
51. Hu, W.; Zhao, T.; Bai, Y.; Shen, L.; Sun, X.; Gu, Y. Contribution of Regional PM_{2.5} Transport to Air Pollution Enhanced by Sub-Basin Topography: A Modeling Case over Central China. *Atmosphere* **2020**, *11*, 1258. [[CrossRef](#)]